Nucleation of cubic boron nitride on boron-doped diamond via plasma enhanced chemical vapor deposition

Jesse M. Brown[a], Saurabh Vishwakarma[b], David J. Smith[a] and Robert J. Nemanich[a]*

[a] Department of Physics, Arizona State University, Tempe, AZ 85287, USA

[b] School for Engineering of Matter, Transport and Energy, Arizona State University, Tempe, Arizona 85287, USA

* Corresponding author: robert.nemanich@asu.edu

Abstract:

Cubic boron nitride (c-BN), with a small 1.4% lattice mismatch with diamond, presents a heterostructure with multiple opportunities for electronic device applications. However, the formation of c-BN / diamond heterostructures has been limited by the tendency to form hexagonal BN at the interface. In this study, c-BN has been deposited on free standing polycrystalline and single crystalline boron doped diamond substrates via electron cyclotron resonance plasma enhance chemical vapor deposition (ECR PECVD), employing fluorine chemistry. In-situ X-ray photoelectron spectroscopy (XPS) is used to characterize the nucleation and growth of boron nitride (BN) films as a function of hydrogen gas flow rates during deposition. The PECVD growth rate of BN was found to increase with increased hydrogen gas flow. In the absence of hydrogen gas flow the BN layer was reduced in thickness or etched. XPS results show that an excess of hydrogen gas significantly increases the percent of sp^2 bonding, characteristic of hexagonal BN (h-BN), particularly during initial layer growth. Reducing the hydrogen flow, such that hydrogen gas is the limiting reactant, minimizes the sp^2 bonding during nucleation of BN. TEM results indicate partial coverage of the diamond with thin epitaxial islands of c-BN. The limited hydrogen reaction is found to be a favorable growth environment for c-BN on boron-doped diamond.

Introduction:

With properties rivaling diamond, the cubic phase of boron nitride (c-BN), with a zinc blende structure, has received much interest as an ultra-wide bandgap semiconductor (~6.4 eV). A high thermal conductivity of ~ 13W/cm K[1], chemical inertness[2], and an oxidation stability up to 1500°C[1] makes c-BN an ideal material as a protective coating in corrosive and thermal environments. With hydrogen termination, c-BN has been shown to have a negative electron affinity (NEA) [3],[4],[5] making it a promising material for thermionic devices. Both p-type and n-type doping have been demonstrated[2]. A predicted high breakdown field (~8-13 MV/cm)[1],[6] would enable application in high power and high frequency devices[7]. Additionally, c-BN can act as an efficient thermal neutron to alpha converter[8],[9]. The thermal neutron absorption cross-section of ^{10}B is one of the largest of all elements (~3840 barns)[10]. Therefore, semiconducting c-BN structures may have potential application as a highly efficient thermal neutron detector.

The first reported synthesis of c-BN was in 1957, where a high-pressure high-temperature (HPHT) process was employed at the GE Research Laboratories[11]. Most reports of c-BN HPHT synthesis describe c-BN crystals ~ 10 -100 μm in diameter, which are used as an abrasive or as a protective layer for cutting tools. A major limitation of using HPHT c-BN for electronics applications is the crystal size, the largest of which have only reached a few millimeters in diameter, which is too small for most electronics applications[2],[6]. High quality thin films of c-BN could be an alternative to bulk c-BN for many electronic applications such as diodes or as a dielectric[12]. An ideal substrate for c-BN thin films is diamond due to its small lattice mismatch of 1.4%, which provides a low stress template for heteroepitaxy. Recent advances in diamond growth technology have provided consistent quality single crystal substrates.

Several physical vapor deposition (PVD) techniques have been successfully used to deposit c-BN thin films since the 1990's[2]. Many previous reports of PVD c-BN on diamond typically produced mixed crystal phases of c-BN and hexagonal boron nitride (h-BN), with an amorphous phase at the growth interface[6]. Thin films of c-BN deposited using PVD require high energy ion bombardment, with accelerating voltages of ~ 300 - 400 V to enable formation of c-BN[13]. The high energy ions (Ar^+, N^+) typically used in PVD of c-BN, can produce films with poor crystallinity, high defect density, and high internal stress, which leads to delamination[2],[6]. Advances in the PVD of c-BN have been able to prevent the mixed crystal phase by precise control of the accelerating voltage[13]. A recent report has shown epitaxial c-BN on (111) diamond using ion beam assisted MBE[14]. This report found that high substrate temperatures (~920°C) yielded epitaxial c-BN on (111) diamond. However, stacking fault defects in the c-BN film were observed, which caused rotated crystal domains, and the formation of the wurtzite phase at the growth interface. The defect density of PVD c-BN remains an issue for its use in electronic applications.

A recent study that used ion assisted MBE found that epitaxial c-BN was preferentially formed on diamond when a trace amount of Mg was present in the deposition system[15]. It was suggested that the Mg could lower the barrier for c-BN formation. In some ways this process has characteristics of chemical vapor deposition.

Alternatively, plasma enhanced chemical vapor deposition (PECVD) relies on surface chemistry for the growth process, which avoids the ion bombardment used in PVD. PECVD has been shown to be effective at producing c-BN films with increased crystalline domain size over PVD[2],[6],[16]. However, the presence of hexagonal boron nitride (h-BN) at the interface inhibits large area heteroepitaxy of c-BN needed for many electronic applications. In fact, h-BN has its

own unique and interesting properties and being able to selectively grow either phase with high purity could be important for specific applications.

The incorporation of fluorine chemistry during the PECVD process provides a chemical mechanism for the preferential etching of h-BN[16],[17]. Atomic fluorine, produced in the plasma, was shown to etch h-BN at a higher rate than c-BN[17],[18]. Moreover, the gas phase ratio of H/F was found to strongly influence the growth rate, and BN phase purity[13]. The PECVD precursor gases of boron trifluoride, nitrogen, and hydrogen, react in the gas phase to form the proposed surface growth reactants of BF_x and NH_x[16],[17],[18]. Previous work on PECVD of BN[3] has shown that substrate bias can also be used to control the phase of the deposited film. For an applied bias below a critical value ($V_{applied} < 40V$) the BN thin films had a majority of h-BN phase. Above this critical bias value, there is a range of bias values ($40V < V_{applied} < 100V$) that produce films, which are predominately c-BN. Increasing the bias further ($V_{applied} > 125V$) results in etching of the deposited film[3]. This present study, which is focused on surface chemical processes, is completed with an applied bias of 60V, which is within the range that is favorable for c-BN growth.

First-principles calculations based on density functional theory have been performed to study the role of hydrogen defects in h-BN and c-BN structures[19]. The results indicate that hydrogen defects in h-BN form between layers with minimal distortion of the local structure. In contrast, hydrogen defects in c-BN are incorporated along B—N bonds, significantly distorting the tetrahedral structure toward a more planar structure, similar to h-BN. These calculations suggest that the incorporation of hydrogen impurities during the nucleation of BN would be beneficial for the formation of h-BN and detrimental to the formation of c-BN.

In this work we investigate the role of gas phase hydrogen on the nucleation and growth of c-BN on diamond using PECVD and fluorine chemistry. Based on the experimental evidence of preferential etching of h-BN by fluorine radicals and the calculations indicating the role of hydrogen defects, we anticipate a trend in the h-BN to c-BN ratio as the hydrogen gas flow is systematically varied. X-ray photoelectron spectroscopy is employed, to characterize the sp^2 or sp^3 bonding of the as-grown thin films, as well as the thickness and growth rates as a function of hydrogen gas flow. High resolution transmission electron microscopy of the initial growth provides insight into the nucleation morphology of the BN layer.

Experiment:

Deposition of boron nitride was performed on boron-doped polycrystalline diamond plates (5mm x 5mm x 0.45mm; doping concentration [B] = 2-6x10^{20} cm^{-3}; supplied by Element Six), in addition to single crystal (1 0 0) boron-doped diamond plates with a 5° offcut (3mm x 3mm x 0.3mm; doping concentration [B] = 2-6x10^{20} cm^{-3}; supplied by TISNCM). Each substrate was mounted on a nichrome (Ni/Cr/Nb) plate with tantalum wires and bound to a molybdenum sample holder. The polycrystalline diamonds have the rough side (R_a~ 50 μm) in contact with the nichrome plate. The smooth side (R_a < 30 nm) is employed as the BN growth surface. The sample holder is placed into the load locked transfer line, an integrated vacuum system with a base pressure of ~5·10^{-9} Torr. Thus, the sample maintains a clean surface or the BN growth surface during *in-vacuo* transfer between the deposition chamber and the surface characterization chamber.

An electron cyclotron resonance (ECR) plasma enhanced chemical vapor deposition (ECR-PECVD) chamber was used for cleaning the substrates and for the deposition of boron nitride - see Figure 1. The cleaning and deposition parameters are listed in Table 1. A 35 cm

diameter stainless steel chamber is pumped by a 25.4 cm diameter Pfeiffer turbomolecular pump (Model: TMU-1600) which maintains a base pressure of ~$3.0 \cdot 10^{-9}$ Torr monitored by a cold cathode gauge. An ASTeX 1500i microwave (2.45 GHz) generator coupled with a magnetic field of ~875 G applied by two ASTeX ECR magnets sustains a plasma. The precursor gas mixture (He / Ar / N_2 / H_2 / BF_3) is introduced below the ECR magnets. The substrate is radiatively heated by a toroidal tungsten coil and monitored with a Mikron M90Q optical pyrometer. During deposition, a negative bias is applied to the substrate and sample holder ($V_{Applied}$ = -60 V). Our prior study[3] , showing changes in the growth of c-BN with sample bias, indicates that the bias affects the ion energy at the sample surface. For the c-BN deposition the ion interactions are dependent on the applied bias and the plasma (particularly the pressure and magnetic field). Consequently, ECR-PECVD studies of BN growth often specify the bias, pressure and magnetic field (60V, 2 x 10^{-4} Torr, and 875 Gauss).

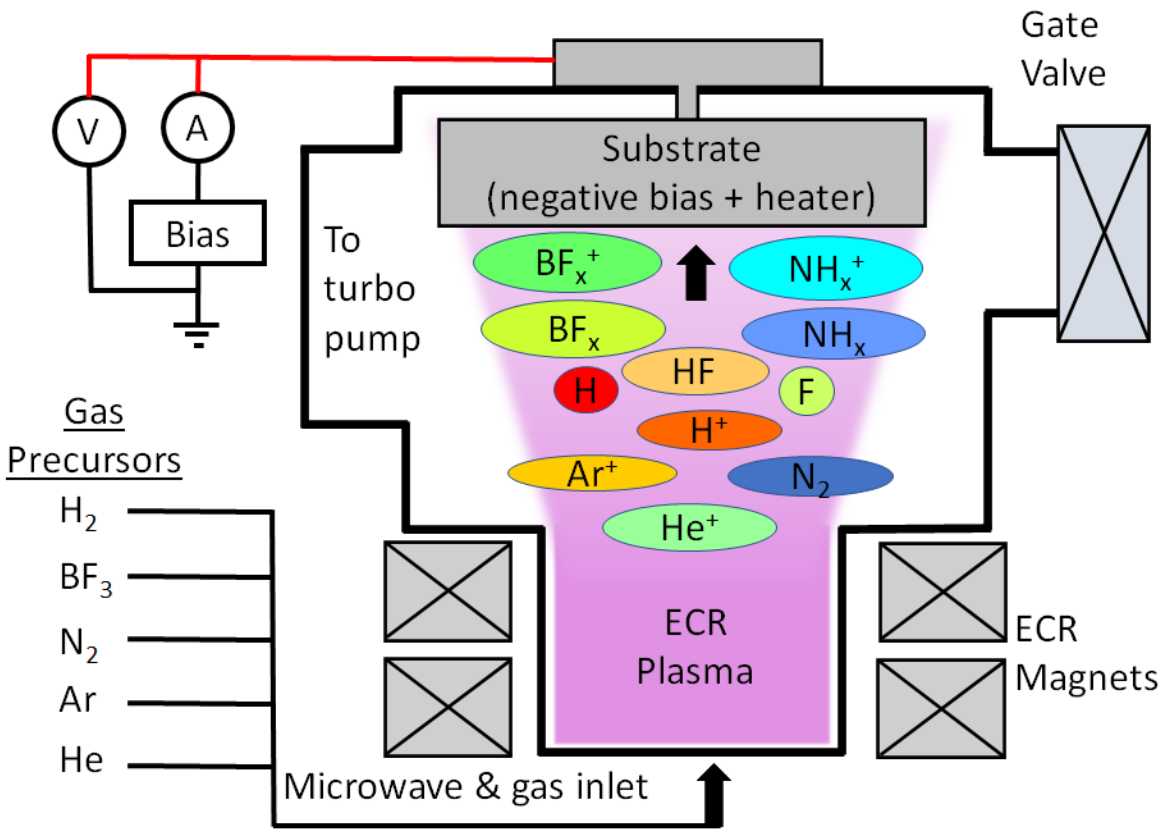

Figure 1. Schematic of the ECR CVD deposition chamber used to deposit boron nitride films. The system employs fluorine chemistry. The colored bubbles indicate the plasma species that contribute to the growth.

	Clean	Deposition
Substrate Temperature	825 ± 25 °C	825 ± 25 °C
Chamber Pressure	2 x 10^{-4} Torr	2 x 10^{-4} Torr
Applied Bias	N/A	-60 V
Deposition Time	30 min at temperature with gas flow + 10 min plasma + cooldown in vacuum	Varied

Gas Flow (sccm)		
He	0	35
Ar	0	2.5
N_2	0	12.5
BF_3	0	1
H_2	20	0,1,2,3,4

Table 1: Experimental parameters for sample cleaning and deposition. Hydrogen plasma is used for cleaning the substrate. The deposition time varies depending on the hydrogen flow and the desired thickness of the film.

In-situ X-ray photoelectron spectroscopy (XPS) is used to analyze the deposited layer surface. The VG-Scienta MX 650 monochromatic Al-Kα x-ray source (1486.6 eV with ΔE of 0.2 eV) is focused to a 7 mm x 2 mm spot size at the sample surface. Each sample is mounted such that the diagonal of the substrate aligns with the elongated X-ray spot to minimize signal from the nichrome mounting plate. The chamber base pressure is $5 \cdot 10^{-10}$ Torr monitored with a hot filament ion gauge. A VG-Scienta R3000 spectrometer with a four-element electrostatic lens is used in sweep mode to scan the full energy range of photoelectrons. The hemispherical analyzer has a slit size of 0.4 mm, and the pass energy is 100 eV giving an energy resolution of 150 meV. The energy resolution of the spectrometer combined with the monochromatic X-ray source, enables a resolution limited FWHM of ~ 0.25 eV. The spectrometer is calibrated using a plasma cleaned gold foil and setting the Au $4f_{7/2}$ peak center at 84.00±0.01 eV.

The XPS spectra are fit with a Tougaard background subtraction, and a sum of Gaussian, and/or Voigt functions using Origin Pro 8.5.1 software. Peak centers correspond to the binding energy (relative to the Fermi level) of the core level electrons, which have characteristic energy ranges depending on the chemical bonding of the element. The integrated peak areas are used to calculate the following quantities:

Thickness of deposited layer[20] $$t = \lambda \cdot \ln\left(\frac{I^S_{C1s}}{I^O_{C1s}}\right) \quad (1)$$

The percent of sp^2 hybridization (h-BN) $$\%sp^2 = 100 \times \frac{I_{B\pi^*}}{I_{B1s}} \Big/ \left(\frac{I_{B\pi^*}}{I_{B1s}}\right)_{Ref} \quad (2)$$

The C 1s peak area of the clean Substrate (I^S_{C1s}), the C 1s peak area after depositing an Overlayer of BN (I^O_{C1s}) and the inelastic mean free path (λ=20.0 Å)[21] of the C 1s photoelectrons traveling through BN are used to calculate the thickness of the deposited film. The π-plasmon ($I_{B\pi^*}$) is characteristic of sp^2 bonding of h-BN. The absence of this peak implies that the film is σ-bonded,

which is a characteristic of sp^3 bonding of c-BN. An h-BN reference sample was prepared by exfoliating a highly ordered pyrolytic BN sample. This sample was used to determine the peak areas, $\left(\frac{I_{B\pi^*}}{I_{B1s}}\right)_{Ref}$ in equation 2. Data presented in Figure 2 has been normalized using the relative atomic sensitivity factors (ASF) {B 1s = 0.13, C 1s = 0.25, N 1s =0.42}[22] to show more clearly the B:N atomic ratio after each process.

The peak fitting procedure was performed systematically throughout. The peak fitting achieved an R^2 of 0.95 or greater indicating the relative areas can be trusted with good reliability. One error mechanism is in the inelastic mean free path. A correction would change the layer thickness but have a lesser effect on the relative concentrations. Assuming a 10 % error in peak intensity and another 10% in the thickness calculation would indicate a 20% uncertainty (for layers less that ~8 nm thickness).

Samples suitable for cross-sectional observation by transmission electron microscopy (TEM) were prepared by focused ion beam (FIB) (Thermo Fisher Scientific, Helios 5 UX dual beam system) initially operated at 30 kV, with further thinning at 5 kV, and at 2 kV. Prior to the FIB process, the surface was coated with amorphous carbon (~100 nm) and W (~2 μm). The FIB process removed a slice of the sample ~10 μm wide x 5 μm deep and ~40 nm thick. The FIB sample enabled examination of ~10 μm of the surface. High-resolution TEM images were recorded using a field emission analytical electron microscope (JEOL, JEM 2010F) operated at 200 kV and with an aberration-corrected TEM (FEI, Titan 80-300) operated at 300 kV.

Results:

In-situ XPS was used to detect and quantify the effects of hydrogen gas flow rates during the growth of c-BN films on diamond using ECR-PECVD and fluorine chemistry. A hydrogen flow of 4 sccm was used to replicate previous work using a similar growth process[3],[23]. An

initial hydrogen plasma (parameters in Table 1) was used to remove air adsorbates and surface oxygen from the boron-doped diamond substrates.

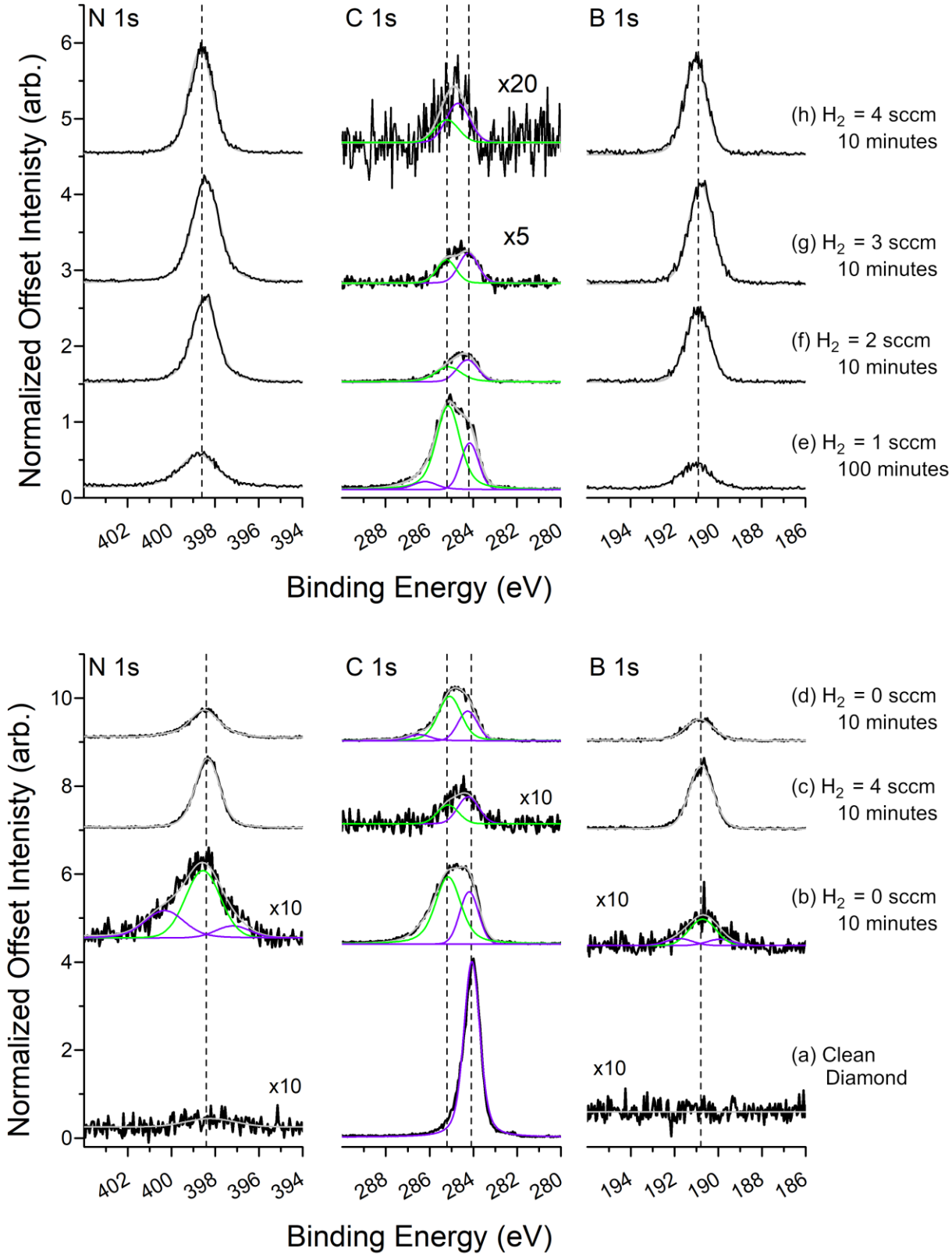
N 1s
C 1s
B 1s
x20
x5
x10
x10
x10
x10
(h) H2 = 4 sccm
10 minutes
(g) H2 = 3 sccm
10 minutes
(f) H2 = 2 sccm
10 minutes
(e) H2 = 1 sccm
100 minutes
(d) H2 = 0 sccm
10 minutes
(c) H2 = 4 sccm
10 minutes
(b) H2 = 0 sccm
10 minutes
(a) Clean
Diamond
Normalized Offset Intenisty (arb.)
Binding Energy (eV)

Figure 2: Evolution of the N 1s, C 1s, and B 1s core energy levels for various hydrogen flow rates. The XPS data has been normalized to the corresponding clean diamond C 1s peak intensity, and the corresponding atomic sensitivity factors to better view the relative concentration of each element. Scans (a)-(d) show the effects of turning the hydrogen gas flow on and off from the same substrate, while scans (e)-(h) show the effects of increasing the hydrogen gas flow on independent substrates.

We first consider the initial growth in Figure 2 comparing scans (a) and (b). The XPS of the clean diamond is shown in Figure 2 scan (a), and the C 1s peak center is at 284.1 eV. This C 1s peak position is consistent with other reports for hydrogen terminated, boron-doped diamond[24],[25],[26]. The hydrogen terminated diamond is then exposed to the ECR-PECVD with deposition parameters indicated in Table 1. The initial deposition was performed with the hydrogen flow turned off (H_2 = 0 sccm), and the XPS results are shown in Figure 2 scan (b). The C 1s peak is significantly broadened relative to the C 1s peak of the clean substrate. The deconvolution of this C 1s peak shows two main components. One peak centered at 285.2 eV, which can be attributed to nitrogen terminated boron doped diamond[26]. The other peak at 284.2 eV is consistent with the initial hydrogen terminated boron-doped diamond.

The N 1s peak is about twice as intense as the B 1s peak. Since the core level scans are corrected for the relative atomic sensitivity factor, the relative intensity of the N 1s and B 1s scans indicates there is ~twice as much nitrogen as boron on the surface. The excess surface nitrogen is interpreted as a nitrogen termination of the diamond surface, with a non-uniform thin BN layer above the nitrogen termination. We assume that the deposited BN is above the nitrogen terminated diamond, and not the hydrogen terminated diamond. Thus, the BN layer thickness is calculated using the area of the deconvoluted peak centered at 285.2 eV in the denominator of Equation (1). The calculated thickness of the BN layer was found to be ~0.3 ± 0.1 nm. The

presence of the BN layer after a deposition with the hydrogen gas flow set to zero suggests that hydrogen is not required to nucleate c-BN on diamond

Extended exposure to the initial growth conditions were further investigated. The $H_2 = 0$ sccm process time was increased from 10 minutes to 100 minutes. There were no observable changes in the XPS results. In particular, the C 1s peak intensity was unaffected. The lack of change in the C 1s peak after an increased process time (10 min. vs 100 min.) indicates that the film thickness was unchanged, and continuous growth is not sustained in the absence of hydrogen.

The effect of introducing hydrogen gas flow is presented in Figure 2 scan (c). The sample initially exposed to the nucleation process (shown in Figure 2 scan (b)) produced a BN thickness of 0.3 nm, was then exposed to the ECR-PECVD deposition with the hydrogen gas flow turned on with a flow rate of 4 sccm (shown in Figure 2 scan(c)). After deposition with hydrogen gas the C 1s peak area is reduced with respect to the C 1s peak area of the clean diamond surface (scans (c) and (a), respectively). The calculated thickness of the BN layer was found to be ~8.8 nm. The assumption that BN is deposited above the nitrogen terminated surface was preserved, and the deconvolved C 1s peak at 285.2 eV was used to calculate the BN thickness. Comparing Figure 2 scan (b) with scan (c) shows the effect that incorporating hydrogen gas during the deposition has on the growth of BN. The deposition times for (b) and (c) are both 10 minutes.

To determine stability of the BN film during the deposition process without hydrogen gas the $H_2 = 0$ sccm process was applied on the 8.8 nm thick BN layer. Figure 2 scan (c) and (d) show the initial 8.8 nm BN layer, and the resulting film after a deposition with $H_2 = 0$ sccm, respectively. The C 1s peak area in Figure 2 scan (d) is significantly increased relative to the C 1s peak area in Figure 2 scan (c). Using the clean diamond C 1s peak area in scan (a) and the C

1s peak area in scan (d), the calculated thickness of the BN layer is found to be ~1.7 nm. The decreased thickness of the BN layer indicates that when hydrogen gas is not included, the plasma etches the BN layer. We consider this to be a significant finding, as it indicates that the hydrogen gas concentration is a critical parameter that controls the reaction equilibrium between etching and growth.

To briefly summarize the results to this point, a polycrystalline diamond substrate was cleaned, Figure 2 scan (a), the substrate was exposed to the ECR-PECVD plasma with the hydrogen off, and results indicated that BN was nucleated while the hydrogen was off, Figure 2 scan (b). The hydrogen was then turned on, and the BN layer began to grow, Figure 2 scan (c). The hydrogen was then turned off again, and the BN layer was partially etched away, Figure 2 scan (d). These results point toward controlling the equilibrium between etching and growth by tuning the hydrogen concentration. Tuning the hydrogen flow such that the etching rate of h-BN is greater than the growth rate, is a strategy to produce an improved c-BN/diamond interface.

To determine the optimum hydrogen gas flow for epitaxial c-BN on diamond, fresh boron-doped polycrystalline substrates were cleaned and exposed to the ECR-PECVD deposition parameters in Table 1 with different hydrogen flow rates (Figure 2 scans (e)-(h)). The BN layer thickness is calculated from the C 1s core level peak at 285.2 eV using each substrate's clean diamond C 1s peak area (centered at 284.2 eV). The deposition using H_2 = 1 sccm, Figure 2 scan (e), resulted in a BN film with a thickness of 1.1 nm. The time for this deposition was 100 minutes while the remaining depositions shown (f)-(h) were for 10 minutes each. To ensure a hydrogen gas flow of H_2 = 1 sccm can sustain the growth of BN, a second sample was produced with an increased deposition time of 150 min, this film produced a BN film ~ 4.1 nm thick, indicated in Figure 3. Put another way the growth rate for 100 min was 0.011 nm/min, and the

growth rate for 150 minutes was 0.027nm/min. Increasing the hydrogen gas flow to H_2 = 2 sccm (f) increased the growth rate to 0.34 nm/min. Further increasing the hydrogen gas flow to H_2 = 3 sccm (g) increased the growth rate to 0.66 nm/min, and finally bringing the hydrogen gas flow to H_2 = 4 sccm (h) increased the growth rate to 0.88 nm/min.

These findings indicate that increasing the hydrogen flow increases the BN growth rate. The BN thickness and growth rates as a function of hydrogen gas flow in the ECR-PECVD plasma are collected in Figure 3. The reaction with H_2 = 1 sccm, Figure 2 scan (e), produced a very thin film. To ensure when hydrogen gas flow of H_2 = 1 sccm can sustain the growth of BN, a second sample was produced with an increased deposition time of 150 min, this film produced a BN film ~ 4.1 nm thick, indicated in Figure 3.

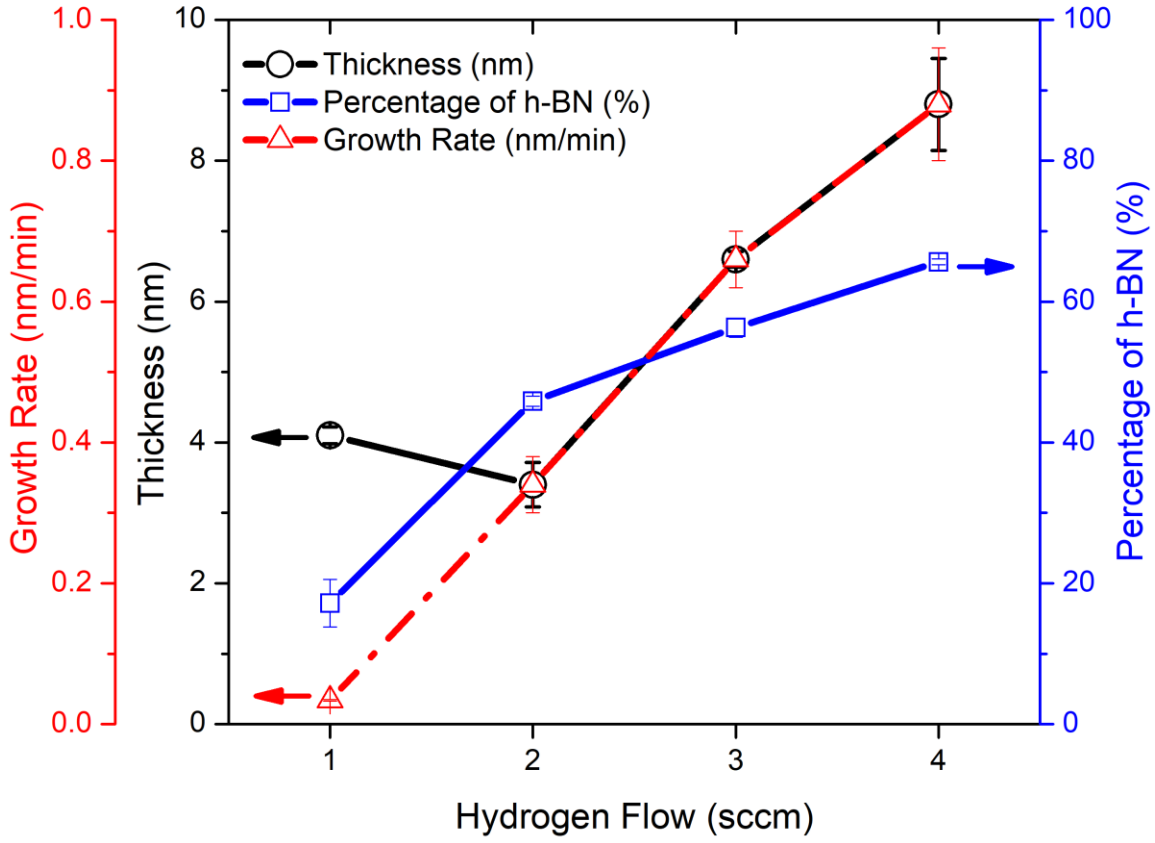

Figure 3: Growth Rates, thickness, and percentage of h-BN as a function of hydrogen flow rates. Due to the slow growth rate with H_2 = 1 sccm, the deposition time shown here was 150 min, while all other flow rates had deposition times of 10 min. Note the correlation between growth rate and percentage of h-BN.

We now consider how the hydrogen gas flow affects the fraction of h-BN produced during the deposition. A closer investigation into the BN film growth using hydrogen gas flows of H_2 = 1 sccm, and H_2 = 2 sccm is shown in Figure 4. The characteristic π-plasmon peak centered at ~200 eV corresponds to π-bonding in h-BN. Using a hydrogen flow of H_2 = 1 sccm for a deposition time of 30 minutes (Figure 4 scan (a)), and 150 minutes (Figure 4 scan (b)) produced BN films of ~0.6 nm and ~4.1 nm, respectively. The deposition with H_2 = 2 sccm for 10 minutes (Figure 4 scan (c)) and 40 minutes (Figure 4 scan (d)) produced BN films of 3.4 nm and greater than 10 nm, respectively. The BN films of Figure 4 (b) and (c) have comparable thicknesses. However, when H_2 = 2 sccm is used, the π-plasmon peak is more pronounced than when H_2 = 1 sccm is used. We note that the B1s binding energy was also related to chemical shifts related to sp^2 or sp^3 bonding [3]. The slightly larger binding energy of scans (b) and (d) is consistent with a larger fraction of sp^3 bonding as noted previously [3].

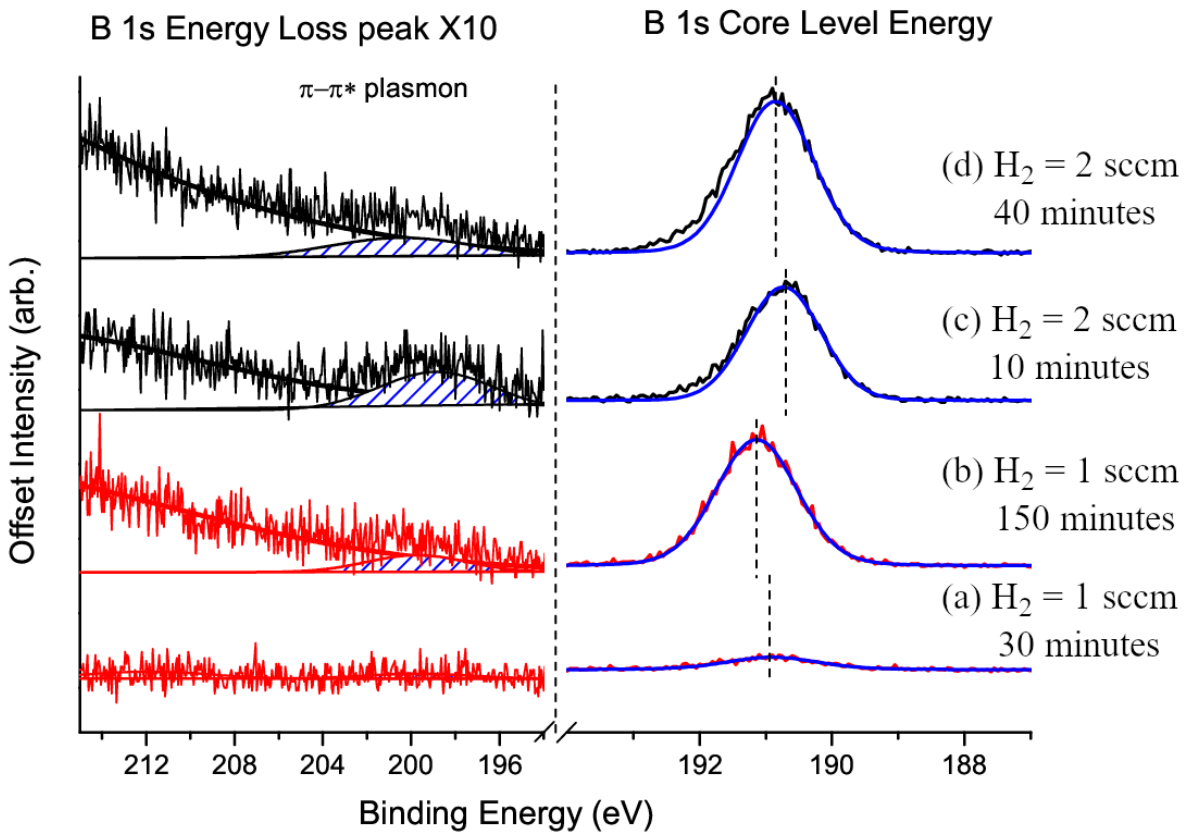

Figure 4: The B 1s core level (right) and enlarged π-plasmon energy loss peak spectrum (left) for BN deposition using limited H2 flow for (a) 30 minutes and (b) for 150 minutes and using excess H_2 flow for (c) 10 minutes and (d) 40 minutes. The results for deposition with a limited H_2 flow show a reduced π-plasmon energy loss peak.

The BN films shown in Figure 4 scans (b) and (d) have comparable intensity of π-plasmon peaks. However, the BN film in Figure 4 scan (d) is much thicker than the BN film in Figure 4 scan (b). The π-plasmon peaks in Figure 4 scans (c) and (d) show that for thicker BN films the intensity of π-plasmon peaks, and consequently, the percentage of h-BN is reduced. This implies that there is a significant fraction of h-BN at the diamond interface that is buried as the c-BN growth begins to dominate after deposition of 10 nm or more of BN. Therefore, by

reducing the hydrogen gas flow from H_2 = 2 sccm to H_2 = 1 sccm, a substantial reduction of the percentage of h-BN at the interface is observed.

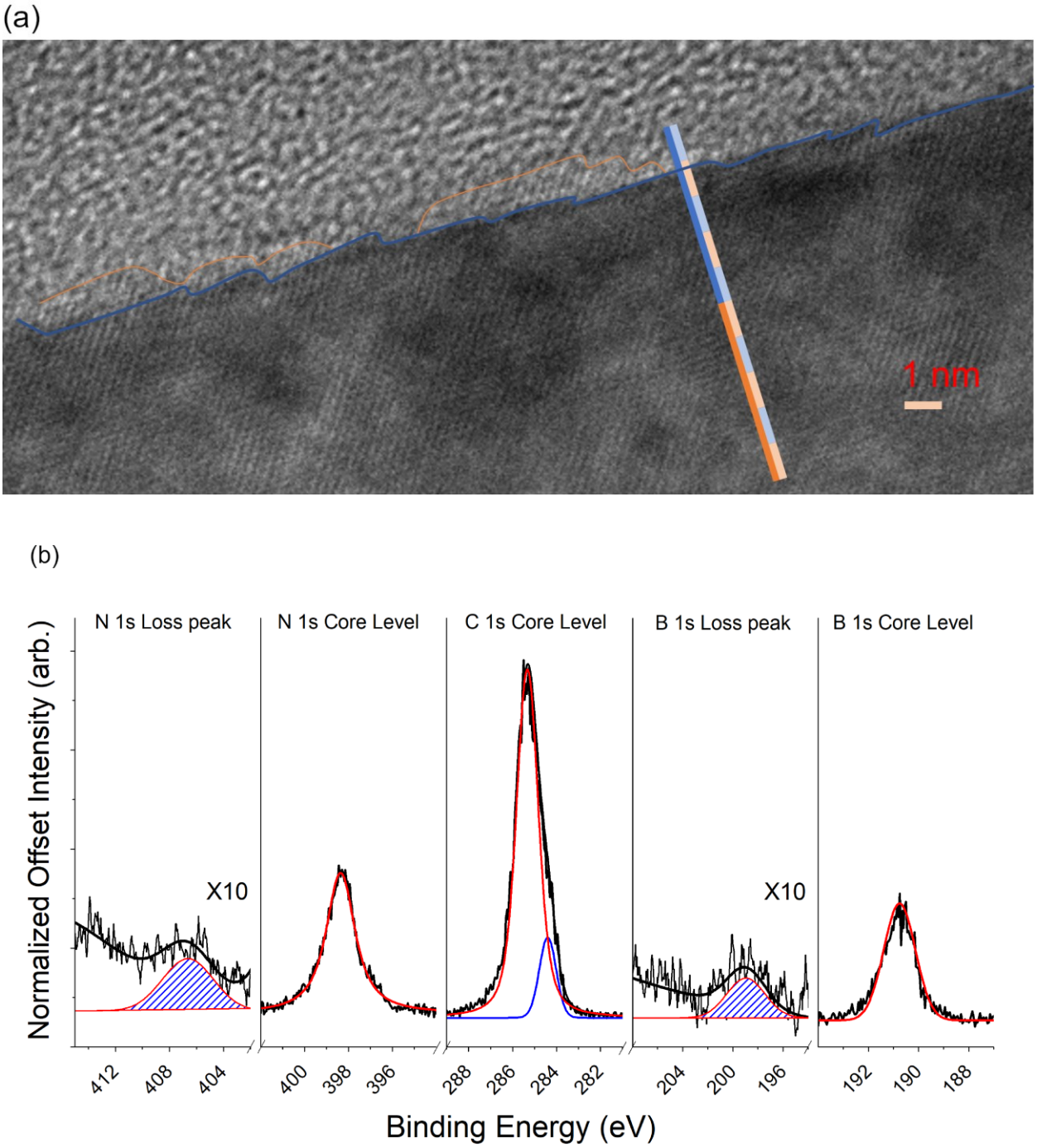

Figure 5: (a) HRTEM image showing nucleation of a very thin, epitaxial layer of c-BN on (100) boron-doped diamond substrate. The stepped diamond surface, and c-BN islands have been

lightly outlined in blue and orange respectively. A scale bar is perpendicular to the surface with 1 nm and 5 nm indicators. (b) The associated XPS spectra.

The initial nucleation of c-BN on a single crystal diamond substrate, characterized with XPS, was prepared for TEM to investigate the film morphology (Figure 5). The BN deposition recipe using a hydrogen gas flow of H_2 = 1 sccm was repeated on a 3 mm x 3 mm single crystal (100) boron-doped diamond (with 5° offcut) substrate. The XPS analysis indicates that the grown film consists of 1.2 nm of 65% c-BN, covering ~ 80% of the surface. Part of the h-BN deduced from the XPS could be growth on the sample holder, since the X-ray spot size was larger than the single crystal substrate and also illuminated the metal mounting plate. The sample was then removed from the vacuum system for TEM sample preparation and observation.

Under TEM inspection, the diamond substrate showed a stepped surface with flat steps. Surface islands of c-BN were visible across the full extent of the 10 μm TEM sample. High resolution TEM images such as Figure 5, established the epitaxial nature of these islands, which had heights of ~ 1-1.5 nm. In addition, bare surface regions and some non-epitaxial islands with much lower density were also observed.

Discussion:

An unusual aspect of the XPS scans is the shape of the C 1s peak after the initial BN growth process. A double carbon peak is most distinct in Figure 2 scan (e) but is also clearly resolved in Figure 2 scans (b), (d), (f), and (g). Hydrogen-terminated highly boron doped diamond is known to have a C 1s core level energy at 284.1 eV[24],[25],[26]. Nitrogen terminated boron-doped diamond has a C 1s core level energy at 285.2 eV[26]. Previous reports of nitrogen-terminated diamond indicate that the C 1s peak shift is due to both band bending and chemical shift effects[27] .

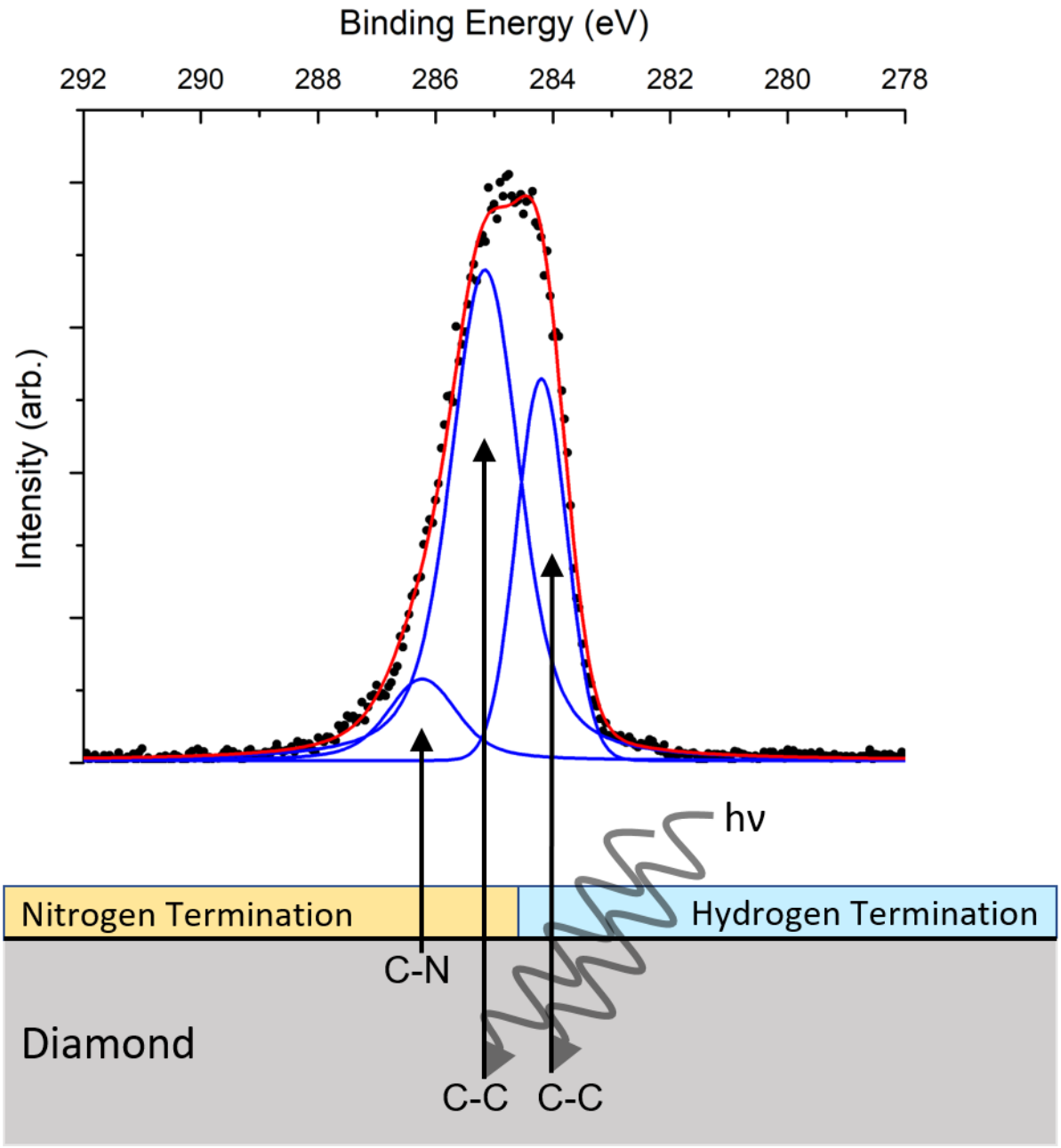

Figure 6: Spectral decomposition of the double C 1s peak from Fig 2(a). The individual spectral components are related to a diamond surface with N- and H-terminated regions. The more intense peaks are related to the C 1s core level energy from the hydrogen terminated surface (284.2 eV) and the C 1s core level energy from the nitrogen terminated diamond surface (285.2 eV). The weaker peak is attributed to carbon - nitrogen bonding near the surface.

For thin layers of BN, both hydrogen-terminated, and nitrogen-terminated C 1s core level peaks are observed as components of the deconvolved peak. A representation of the various diamond terminations, and the carbon bonding configurations within the diamond near surface region are shown in Figure 6. The greater part of the C 1s peak area can be attributed to C—C bonds of the diamond, with the two main peaks attributed to nitrogen-terminated and hydrogen-terminated surface regions [26],[27]. A weaker peak can be attributed to the chemical shift of carbon-nitrogen bonds (C—N)[26],[27].

The double carbon peak is most pronounced for sub-nanometer BN layers (see Figure 2 scan (b) and (e)). The relative intensity of the normalized N 1s peak and B 1s peak for these < 2 nm BN layers are also clearly different. The normalization of the XPS data with the atomic sensitivity factor allows the data to be viewed in a way that presents the atomic ratio of boron to nitrogen (B:N). For very thin (<2 nm) BN layers, the B:N is consistently nitrogen rich (B:N < 0.5). The nitrogen termination of the diamond surface provides an explanation for the B:N ratio shifting to nitrogen rich values for these thin films. As the film thickness increases the B:N trends to 1 as is expected for stoichiometric BN. The thickness calculations quoted in this study assume that the BN formation is occurring above the nitrogen-terminated surface. Therefore, the C 1s peak at 285.2 eV is used to calculate the BN thickness. While the peak at 284.2 eV is used to calculate the percent of the substrate with a hydrogen-terminated surface. The BN thickness and growth rate, for different hydrogen gas flow processes are shown in Figure 3.

The TEM image shown in Figure 5 indicates incomplete coverage of c-BN, further reinforcing the XPS analysis correlating the double carbon peak with a partially covered diamond surface. The C 1s spectra shows a double carbon peak with one peak centered at 284.4 eV ascribed to the hydrogen-terminated diamond substrate surface and the other peak at 285.3

eV ascribed to the diamond substrate surface that is covered by c-BN. The ratio of the peak areas indicates that approximately 80% of the diamond surface is covered with BN, and therefore approximately 20% of the surface is uncovered with BN. The partial coverage is also apparent in the TEM image.

The NH_x and BF_x species formed in the plasma react on the substrate surface to form solid BN and molecular HF[18]. From the results shown in Figure 2 scans (a)-(d), the ECR-PECVD process was performed while the hydrogen gas was turned off and on, and off again. When no hydrogen was used during the ECR-PECVD process, the thin film of BN was etched. Increasing the hydrogen flow from 0 sccm to 1 sccm causes the surface chemistry to switch from etching to growth. Increasing it further to 2 sccm increases the growth rate, and this trend continues for flows of 3 sccm and 4 sccm (Figure 2 scans (d)-(h)). These results indicate that hydrogen enables deposition of BN using PECVD while employing fluorine chemistry. Furthermore, the hydrogen gas flow can be used to control the nucleation and growth rate of BN using ECR-PECVD employing fluorine chemistry.

Another trend that is observed is the correlation between the growth rate and the fraction of h-BN observed in the film. For higher growth rates, the deposited film showed a greater fraction of h-BN. For lower growth rates, the relative growth of c-BN was favored (see Figure 3 and Figure 4). The incorporation of fluorine chemistry has been shown to selectively etch h-BN[18]. If an excess of hydrogen gas is supplied during the deposition, the excess hydrogen at or near the surface may reduce the effectiveness of fluorine chemistry to selectively etch the h-BN. This trend is evident in the balanced chemical Equation (3), which describes the growth mechanism proposed by Zhang and colleagues [18]. Assuming excess N_2, the addition of hydrogen will reduce the concentration of atomic fluorine in the plasma, as seen in Equation (4).

Reducing the hydrogen flow such that hydrogen is the limiting reactant increases the concentration of atomic fluorine, as indicated in Equation (5). A higher concentration of atomic fluorine increases the etching efficiency of h-BN, and enables the formation of higher purity c-BN.

Balanced: $1.5H_2 + BF_3 + N_2 \rightleftarrows BF_x + NH_x + HF \rightleftarrows BN_{(s)} + (x+1)HF$ (3)

Excess H_2: $2H_2 + BF_3 + N_2 \rightleftarrows BF_x + NH_x + HF \rightleftarrows BN_{(s)} + (x+1)HF + H$ (4)

Limited H_2: $1H_2 + BF_3 + N_2 \rightleftarrows BF_x + NH_x + HF \rightleftarrows BN_{(s)} + (x+1)HF + F$ (5)

During PECVD of BN, the influence of the hydrogen gas flow on the c-BN purity is shown in Figure 3. The deposition with a limited hydrogen gas flow (H_2 = 1 sccm) produced a 4.1 nm film, and a small π-plasmon peak (Figure 4 scan (b)), which corresponded to ~17% h-BN. Therefore, most of the deposited film is c-BN. A deposition with an excess hydrogen gas flow (H_2 = 2 sccm) produced a 3.4 nm film with the characteristic π-plasmon peak of h-BN (Figure 4 scan (c)) corresponding to ~62% h-BN. A previous study of BN thin films deposited using PECVD with excess hydrogen gas flow reported a 4.3 nm film with ~68% h-BN[23]. The limited hydrogen gas reaction emphasizes c-BN formation during nucleation on boron-doped diamond.

The concentration of H_2 gas during growth has several effects, not only in the gas phase chemistry that creates the active growth species responsible for h- and c-BN phases and varied growth rates[18],[28], but also the structural properties of the film[19]. As hydrogen ions, atoms, and gas are present during the deposition of BN, as well as a key component of the growth being NH_x, there are several pathways in which the incorporation of hydrogen defects can occur during

the deposition of BN via ECR-PECVD. Theoretical calculations studied the incorporation of hydrogen defects in BN and how the local structure can be perturbed[19].

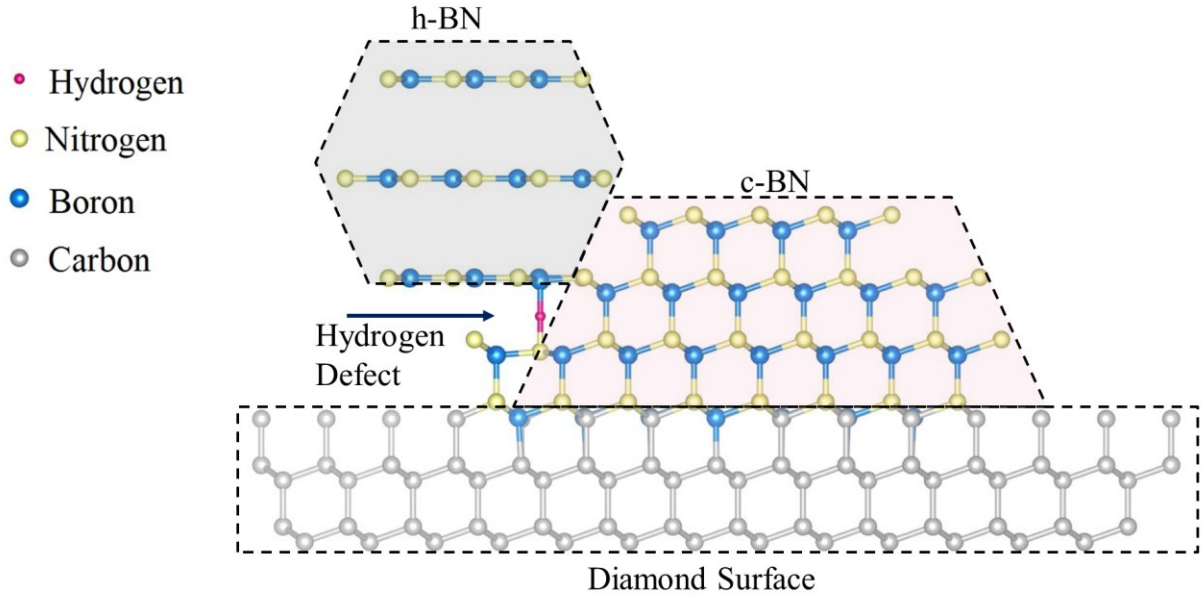

Figure 7: Model of hydrogen defect in c-BN nucleation for the (111) interface. The extra enthalpy of the hydrogen defect causes the N—B bond to increase in length, changing the nearest neighbor bonding angle from isotropic 109° to anisotropic 119° and 94.5°. The incorporation of hydrogen defects can provide a nucleation points for h-BN during the initial stages of c-BN growth.

The theory research suggests that the hydrogen defects in h-BN form between layers with minimal distortion of the local structure[19]. In contrast, hydrogen defects in c-BN form along the B—N bond center, which forces the tetrahedral structure to distort toward a more trigonal pyramidal structure. Based on the calculations provided by D. Han et al[19], we hypothesize the incorporation of a hydrogen defect during the nucleation of c-BN schematically in Figure 7. According to simulations, a hydrogen atom placed at a B—N bond center increases the B—N bond length by 52%[19] and changes the nearest neighbor bond angles from tetrahedral 109° to anisotropic 119° and 94.5°. Notice that the nitrogen atom below the hydrogen is mostly aligned

with the plane of boron atoms instead of the plane of nitrogen atoms. Similarly, the hydrogen defect will perturb the boron atom from the ideal tetrahedral structure into a nearly planar hexagonal structure.

While hydrogen gas can introduce defects that can distort the c-BN to h-BN and stabilize the h-BN phase, it is necessary for continued growth. In the above chemical Equations (4) and (5), the difference between excess hydrogen and limited hydrogen reactions is a relatively small change in the H_2 concentration. For the reaction with a limited hydrogen flow, an excess of fluorine may be anticipated, which could react with h-BN as it is forming. The anticipated excess fluorine may be expected to etch the sp^2 bonded atoms before being buried. Limited hydrogen gas will also minimize hydrogen incorporation in BN thin films, preventing the formation of h-BN nucleation sites, as represented in Figure 7.

Conclusions:

The effect of hydrogen concentration on the growth of boron nitride using ECR PECVD with fluorine chemistry was investigated. To determine the optimum concentration of H_2 for the growth of c-BN, the hydrogen gas flow was varied (0, 1, 2, 3, 4 sccm), while keeping constant temperature, pressure, bias, and other gas flows. This experiment found that hydrogen is a necessary reactant, as continuous growth was not observed in its absence. The growth rate of the BN film can be controlled by tuning the hydrogen to fluorine ratio. The hydrogen flow rate can also be varied to change the proportion of h-BN or c-BN in the film. Excess hydrogen will favor the growth of h-BN, while limited concentration will favor the growth of c-BN. The growth processes [14],[12], selective etching with fluorine, and incorporation of hydrogen defects[16] are considered to discuss the role hydrogen has on the structural properties of the deposited boron

nitride film. We conclude that limiting the hydrogen gas flow provides a more favorable environment for c-BN nucleation and growth. Further research may investigate the use of the limited hydrogen reaction to promote c-BN nucleation, and once a sufficient thickness has formed, increasing the hydrogen to increase the growth rate while maintaining c-BN growth.

Acknowledgments

This work was supported by ULTRA, an Energy Frontier Research Center funded by the U.S. Department of Energy (DOE) Office of Science, Basic Energy Sciences (BES) under Award No. DE-SC0021230 for measurement of the c-BN nucleation, and the National Science Foundation (NSF) under Award No. 2003567 for establishing the surface chemistry effects, and Northrop Grumman University Industrial Affiliates Program for equipment development and testing. Use of facilities in the John M. Cowley Center for High Resolution Electron Microscopy is also acknowledged.

References:

[1] W. Zhang, Y.M. Chong, B. He, I. Bello, S.-T. Lee, Cubic Boron Nitride Films, in: Comprehensive Hard Materials. Elsevier, pp. 607–639 (2014). https://doi.org/10.1016/B978-0-08-096527-7.00061-1

[2] X. Zhang, J. Meng, Recent progress of boron nitrides, in: Ultra-Wide Bandgap Semiconductor Materials, Elsevier, pp. 347–419 (2019). https://doi.org/10.1016/B978-0-12-815468-7.00004-4

[3] J. Shammas, T. Sun, F.A.M. Koeck, A. Rezikyan, R.J. Nemanich, In situ photoelectron spectroscopic characterization of c-BN films deposited via plasma enhanced chemical vapor deposition employing fluorine chemistry, Diamond and Related Materials 56, 13–22 (2015). https://doi.org/10.1016/j.diamond.2015.04.002

[4] Y. Yang, T. Sun, J. Shammas, M. Kaur, M. Hao, R.J. Nemanich, Electron affinity of cubic boron nitride terminated with vanadium oxide, Journal of Applied Physics 118, 165310 (2015). https://doi.org/10.1063/1.4934508

[5] M.J. Powers, L.M. Benjamin, L.M. Porter, R.J. Nemanich, R.F. Davis, J.J. Cuomo, G.L. Doll, S.J. Harris, Observation of a negative electron affinity for boron nitride, Applied Physics Letters 67, 3912 (1998). https://doi.org/10.1063/1.115315

[6] W.J. Zhang, I. Bello, Y. Lifshitz, S.T. Lee, , Recent Advances in Cubic Boron Nitride Deposition. MRS Bulletin 28, 184–188 (2003). https://doi.org/10.1557/mrs2003.60

[7] Y. Kumashiro, S. Shikata, N. Fujimori, Semiconducting Diamond and Diamond Devices, in: Electric Refractory Materials, p385 (2000) (Marcel Dekker, New York). https://doi.org/10.1201/9780203908181

[8] J. Holmes, J. Brown, F.A. Koeck, H. Johnson, M.K. Benipal, P. Kandlakunta, A. Zaniewski, R. Alarcon, R. Cao, S.M. Goodnick, R.J. Nemanich, Performance of 5- μm PIN diamond diodes as thermal neutron detectors, Nuclear Instruments and Methods in Physics Research Section A: Accelerators, Spectrometers, Detectors and Associated Equipment 961, 163601 (2020). https://doi.org/10.1016/j.nima.2020.163601

[9] J. Holmes, M. Dutta, F.A. Koeck, M. Benipal, J. Brown, B. Fox, R. Hathwar, H. Johnson, M. Malakoutian, M. Saremi, A. Zaniewski, R. Alarcon, S. Chowdhury, S.M. Goodnick, R.J. Nemanich, A 4.5 μm PIN diamond diode for detecting slow neutrons, Nuclear Instruments and

Methods in Physics Research Section A: Accelerators, Spectrometers, Detectors and Associated Equipment 903, 297–301 (2018). https://doi.org/10.1016/j.nima.2018.06.061
[10] G.F. Knoll, Radiation Detection and Measurement, 3rd ed (John Wiley & Sons, Inc., New York, 2000).
[11] R.H. Wentorf, Cubic Form of Boron Nitride, Journal of Chemical Physics 26, 956–956 (1957). https://doi.org/10.1063/1.1745964
[12] T.-H. Yang, J. Brown, K. Fu, J. Zhou, K. Hatch, C. Yang, J. Montes, X. Qi, H. Fu, R.J. Nemanich, Y. Zhao, AlGaN/GaN metal–insulator–semiconductor high electron mobility transistors (MISHEMTs) using plasma deposited BN as gate dielectric, Applied Physics Letters 118, 072102 (2021). https://doi.org/10.1063/5.0027885
[13] K. Hirama, Y. Taniyasu, S.-I. Karimoto, Y. Krockenberger, H. Yamamoto, Single-crystal cubic boron nitride thin films grown by ion-beam-assisted molecular beam epitaxy, Applied Physics Letters 104, 092113 (2014). https://doi.org/10.1063/1.4867353
[14] K. Hirama, Y. Taniyasu, H. Yamamoto, K. Kumakura, Structural analysis of cubic boron nitride (111) films heteroepitaxially grown on diamond (111) substrates, Journal of Applied Physics 125, 115303 (2019). https://doi.org/10.1063/1.5086966
[15] D.J. Storm, S.I. Maximenko, A.C. Lang, N. Nepal, T.I. Feygelson, B.B. Pate, C.A. Affouda, D.J. Meyer, Mg-Facilitated Growth if Cubic Boron Nitride by Ion Beam-Assisted Molecular Beam Epitaxy, Phys. Status Solidi RRL 16, 2200036 (2022). https://doi.org/10.1002/pssr.202200036
[16] W.J. Zhang, I. Bello, Y. Lifshitz, K.M. Chan, Y. Wu, C.Y. Chan, X.M. Meng, S.T. Lee, Thick and adherent cubic boron nitride films grown on diamond interlayers by fluorine-assisted chemical vapor deposition, Applied Physics Letters 85, 1344–1346 (2004). https://doi.org/10.1063/1.1784545
[17] W.J. Zhang, S. Matsumoto, The roles of hydrogen and fluorine in the deposition of cBN films with the Ar_N_2_BF_3_H_2 system, Chemical Physics Letters 330, 243–248 (2000).
[18] W.J. Zhang, C.Y. Chan, X.M. Meng, M.K. Fung, I. Bello, Y. Lifshitz, S.T. Lee, X. Jiang, The Mechanism of Chemical Vapor Deposition of Cubic Boron Nitride Films from Fluorine-Containing Species, Angewandte Chemie International Edition 44, 4749–4753 (2005). https://doi.org/10.1002/anie.200500320

[19] D. Han, X.-B. Li, Y.Y. Sun, S.B. Zhang, S.-Y. Xie, S. Limpijumnong, Z.-G. Chen, H.-B. Sun, Role of hydrogen in the growth of boron nitride: Cubic phase versus hexagonal phase, Computational Materials Science 82, 310–313 (2014). https://doi.org/10.1016/j.commatsci.2013.09.065

[20] A. Jablonski, J. Zemek, Overlayer thickness determination by XPS using the multiline approach: Overlayer thickness determination by XPS using the multiline approach, Surface and Interface Analysis 41, 193–204 (2009). https://doi.org/10.1002/sia.3005

[21] H. Shinotsuka, S. Tanuma, C.J. Powell, D.R. Penn, Calculations of electron inelastic mean free paths. XII. Data for 42 inorganic compounds over the 50 eV to 200 keV range with the full Penn algorithm, Surf Interface Anal 51, 427–457 (2019). https://doi.org/10.1002/sia.6598

[22] C.D. Wagner, L.E. Davis, M.V. Zeller, J.A. Taylor, R.H. Raymond, L.H. Gale, Empirical atomic sensitivity factors for quantitative analysis by electron spectroscopy for chemical analysis, Surf. Interface Anal. 3, 211–225 (1981). https://doi.org/10.1002/sia.740030506

[23] J. Shammas, Y. Yang, X. Wang, F.A.M. Koeck, M.R. McCartney, D.J. Smith, R.J. Nemanich, Band offsets of epitaxial cubic boron nitride deposited on polycrystalline diamond via plasma-enhanced chemical vapor deposition, Applied Physics Letters 111, 171604 (2017). https://doi.org/10.1063/1.5009089

[24] S. Ghodbane, D. Ballutaud, A. Deneuville, C. Baron, Influence of boron concentration on the XPS spectra of the (100) surface of homoepitaxial boron-doped diamond films, Physica Status Solidi (a) 203, 3147–3151 (2006). https://doi.org/10.1002/pssa.200671123

[25] L. Diederich, O.M. Küttel, P. Ruffieux, T. Pillo, P. Aebi, L. Schlapbach, Photoelectron emission from nitrogen- and boron-doped diamond (100) surfaces, Surface Science 417, 41–52 (1998). https://doi.org/10.1016/S0039-6028(98)00638-4

[26] A. Denisenko, A. Romanyuk, L.A. Kibler, E. Kohn, Surface structure and electrochemical characteristics of boron-doped diamond exposed to rf N_2-plasma, Journal of Electroanalytical Chemistry 657, 164–171 (2011). https://doi.org/10.1016/j.jelechem.2011.04.021

[27] M. Attrash, M.K. Kuntumalla, A. Hoffman, Bonding, structural properties and thermal stability of low damage RF (N_2) plasma treated diamond (100) surfaces studied by XPS, LEED, and TPD. Surface Science 681, 95–103 (2019). https://doi.org/10.1016/j.susc.2018.11.006

[28] C. Chan, W.J. Zhang, X.M. Meng, K.M. Chan, I. Bello, Y. Lifshitz, S.T. Lee, The growth of thick cBN films employing fluorine chemistry and ECR deposition, Diamond and Related Materials 12, 1162–1168 (2003). https://doi.org/10.1016/S0925-9635(02)00288-1